The optical Tamm states at the edges of a photonic crystal bounded by one or two layers of a strongly anisotropic nanocomposite

S. Ya. Vetrov[1,2], R. G. Bikbaev[1,*], and I. V. Timofeev[1,2]

[1]*Siberian Federal University, Krasnoyarsk, 660041 Russia*
[2]*Kirensky Institute of Physics, Russian Academy of Sciences, Siberian Branch, Krasnoyarsk, 660036 Russia*
Corresponding author: rashid-bikbaev@mail.ru

The optical Tamm states localized at the edges of a photonic crystal bounded by a nanocomposite on its one or both sides are investigated. The nanocomposite consists of metal nanoinclusions with an orientation-ordered spheroidal shape, which are dispersed in a transparent matrix, and is characterized by the effective resonance permittivity. The spectrum of transmission of the longitudinally and transversely polarized waves by such structures at the normal incidence of light was calculated. The spectral manifestation of the Tamm states caused by negative values of the real part of the effective permittivity in the visible spectral range was studied. Features of the spectral manifestation of the optical Tamm states for different degrees of extension of spheroidal nanoparticles and different periods of a photonic crystal were investigated. It is demonstrated that splitting of the frequency due to elimination of degeneracy of the Tamm states localized at the interfaces between the photonic crystal and nanocomposite strongly depends on the volume fraction of the spheroids in the nanocomposite and on the ratio between the polar and equatorial semiaxes of the spheroid. Each of the two orthogonal polarizations of the incident wave has its own dependence of splitting on the nanoparticle density, which makes the transmission spectra polarization-sensitive. It is shown that the Tamm state is affected by the size-dependent permittivity of anisotropic nanoparticles.

1. INTRODUCTION

The surface electromagnetic states in photonic-crystal structures have been attracting attention of researches for a long time [1]. In recent years, there has been an increased interest in a special type of the localized electromagnetic states excited at the normal incident that are called the optical Tamm states (OTSs) [2]. Such states are analogous to the Tamm surface states in physics of condensed matter. They can be excited between two different photonic crystals with overlapping band gaps [3] or between a photonic crystal and a medium with negative permittivity ε [4, 5]. The surface electromagnetic wave at the interface between the photonic crystal and the medium with ε < 0 is a single unit with the surface plasmon, i.e., oscillations of free electrons near the conductor surface. In experiments, the OTS manifests itself as a narrow peak in the transmission spectrum of a sample [6, 7].

Surface modes and OTSs can be used in sensors and optical switches [8], multichannel filters [9], Faraday- and Kerr-effect amplifiers [7, 10], organic solar cells [11], and absorbers [12]. The authors of study [13] experimentally demonstrated a laser based on the Tamm structure consisting of quantum wells embedded in a Bragg reflector with the silver-coated surface. Gazzano et al. experimentally showed the possibility of implementation of a single-photon source on the basis of confined Tamm plasmon modes [14]. The optical Tamm states in magnetophotonic crystals were investigated in studies [7, 15−17]. Resonance hybrid states arise as a result of removal of degeneracy in the interaction of two or more different modes with the same frequency. The hybrid states were studied in [18−21]. In [22], the electro-optically tunable Tamm plasmon exciton polaritons were investigated. The authors of [23] predicted that the edges of a finite one-dimensional array of dielectric nanoparticles with the high refractive index can sustain the damped OTSs. The authors of [24] proposed and implemented the extremely high-efficiency transmission of light through a nanohole in a gold film, which was placed in the light field localized at the interface between the film and a one-dimensional photonic crystal. This effect is related to the field amplification at the interface between the superlattice and the metal film due to the occurrence of the OTS. The authors of [25] disclosed the surface state in the structure containing a cholesteric liquid crystal and showed that the condition for its existence is the presence of a quarter-wavelength layer between the crystal and metal, which is explained by the polarization properties of cholesterics different from the properties of scalar structures.

The aim of this study was to investigate the properties of the OTSs localized at the edges of a photonic crystal bounded by a nanocomposite with the strongly anisotropic effective permittivity on one or both sides. The strong anisotropy is due to the strongly extended or flattened spheroids. We demonstrate that the interaction between Tamm plasmons localized at the interfaces between the PC and nanocomposite leads to splitting of modes, which significantly depends on the fraction of metal nanoinclusions in the latter. We consider the correlation between the size effect and formation of the Tamm states.

2. DESCRIPTION OF THE MODEL AND DETERMINATION OF TRANSMISSION

The investigated PC structure is a layered medium bounded by finite nanocomposite media on one or both sides (Fig. 1). A unit cell of the PC is formed from materials a and b with respective layers thicknesses d_a and d_b and permittivities ε_a and ε_b. The

nanocomposite layer with thickness d_{mix} consists of metal nanoparticles in the form of ellipsoids of revolution (spheroids) uniformly distributed in the dielectric matrix and oriented along the axis of revolution coinciding with the x axis.
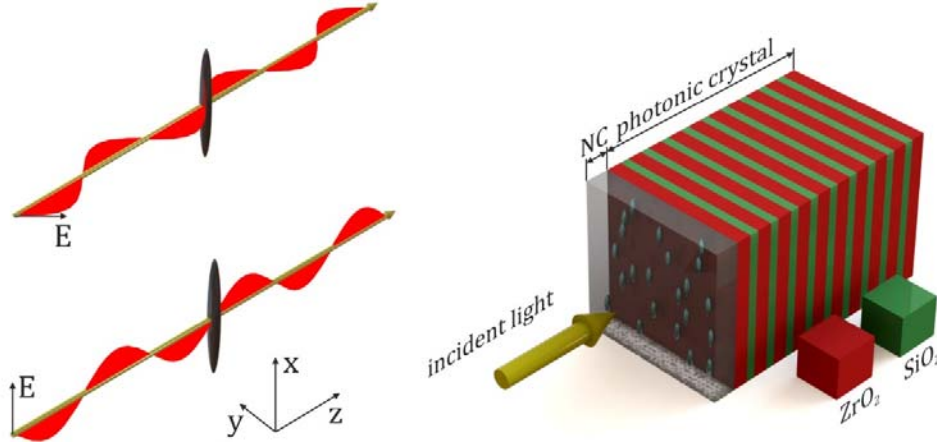

Fig. 1. Schematic of the 1D PC conjugated with the anisotropic nanocomposite layer.

Here in after, we consider the PC structure to be placed in vacuum. The effective permittivity of the nanocomposite with the properties of a uniaxial substance is presented in the principle axes as a diagonal tensor with the components $\varepsilon_{xx} = \varepsilon_{II}$ and $\varepsilon_{yy} = \varepsilon_{zz} = \varepsilon$. The effective permittivity of the nanocomposite is determined from the Maxwell−Garnett formula [26] widely used in study of the matrix media in which a small fraction of isolated metal inclusions is dispersed in a material. The formula is

$$\varepsilon_{\perp,\parallel} = \varepsilon_d \left[1 + \frac{f(\varepsilon_m - \varepsilon_d)}{\varepsilon_d + (1-f)(\varepsilon_m - \varepsilon_d)L_{\perp,\parallel}} \right] \tag{1}$$

where f is the filling factor, i.e., the fraction of nanoparticles in the matrix; ε_d and $\varepsilon_m(\omega)$ are the permittivities of the matrix and nanoparticle metal, respectively; and ω is the radiation frequency. Depolarization factors $L_{\perp,\parallel}$ in formula (1) depend on the ratio between lengths a and b of the polar and equatorial semiaxes of the spheroid and on the field direction. For the field directed along the axis of revolution of the spheroid, factor $L_{\parallel}$ is determined as

$$L_{\parallel} = \frac{1}{1-\xi^2} \left(1 - \xi \frac{\arcsin\sqrt{1-\xi^2}}{\sqrt{1-\xi^2}} \right) \tag{2}$$

For the field directed perpendicular to the axis of revolution of the spheroid, the factor is

$$L_{\perp} = (1 - L_{\parallel})/2 \tag{3}$$

Where $\xi = a/b$. The case $\xi<1$ corresponds to the flattened spheroid and the case $\xi>1$, to the extended spheroid. The case $\xi = 1$, when we have $L_{\perp} = L_{\parallel} = 1/3$ and $\varepsilon_{\parallel} = \varepsilon_{\perp} = \varepsilon_{mix}$, corresponds to the sphere.
The Maxwell−Garnett model suggests the quasi-classical approximation and has the following characteristics: (i) the nanocomposite layer is electrodynamically isotropic, (ii) size of the inclusions in the dielectric matrix of the nanocomposite and the distance between the inclusions are small compared to the optical wavelength in the effective medium. The predictions of the Maxwell−Garnett model for the effective medium are reliable for a moderate fraction of inclusions with the filling factor $0.01 < f < 0.3$ [27]. The technology for fabricating such nanocomposites with silver nanoparticles of the required shape and orientation in a glass matrix was described in [28, 29].
We find the permittivity of the nanoparticle metal using the Drude approximation

$$\varepsilon_m(\omega) = \varepsilon_0 - \frac{\omega_p^2}{\omega(\omega + i\gamma)} \tag{4}$$

here ε_0 is the constant that takes into account the contribution of interband transitions of bound electrons, ω_p is the plasma frequency, and γ is the reciprocal electron relaxation time. Transmission of a planar acoustic wave polarized along the x axis and propagating along the z direction was calculated using the transfer matrix technique [30]. The variation in the light field upon

transmission through each structure layer is determined by the second-order transfer matrix. The transfer matrix of the entire structure that relates the amplitudes of the incident and transmitted waves is a product of 2 x 2 matrices

$$M = T_{01}T_{02} \ldots T_{N-1,N}T_{N,S} \tag{5}$$

where the transfer matrix is

$$T_{n-1,n} = \frac{1}{2}\begin{pmatrix} (1+h)e^{-i\alpha_n\gamma_n} & (1-h)e^{i\alpha_n\gamma_n} \\ (1-h)e^{-i\alpha_n\gamma_n} & (1+h)e^{i\alpha_n\gamma_n} \end{pmatrix} \tag{6}$$

Here, $h=(\varepsilon_n/\varepsilon_{n-1})^{1/2}$, $\varepsilon(n)$ is the permittivity of the n layer, $\alpha=(\omega/c)\varepsilon(n)^{1/2}$, ω is the wave frequency, c is the speed of light, and $\gamma_n = z_n - z_{n-1}$ is the layer thicknesses, where $n = 1,2,\ldots, N$ and z_n is the coordinate of the interface between the n layer and the $(n + 1)$ layer adjacent from the right ($\gamma_{N+1} = 0$). The transfer matrix for the orthogonally polarized wave is obtained from Eq. (6) by substituting $(\varepsilon_{n-1}/\varepsilon_n)^{1/2}$ for h. The energy transmittance, reflectance, and absorbance are determined using the respective formulas

$$T(\omega) = \frac{1}{\left|\hat{M}_{11}\right|^2}, R(\omega) = \frac{\left|\hat{M}_{11}\right|^2}{\left|\hat{M}_{21}\right|^2} \tag{7}$$

$$A(\omega) = 1 - T(\omega) - R(\omega) \tag{8}$$

Here, M_{11} and M_{21} are the elements of matrix M.

3. RESULTS AND DISCUSSION

3.1. Optical Tamm plasmon polaritons at the interface between the PC and strongly anisotropic nanocomposite layer

For certainty, we will investigate zirconium dioxide ZrO_2 with the permittivity $\varepsilon_a = 4.16$ and silicon dioxide SiO_2 with the permittivity $\varepsilon_b = 2.10$ as materials of the alternating PC layers. The layer thicknesses are $d_b = 50$ nm and $d_a = 74$ nm and the number of layers is $N = 21$.

The dielectric nanocomposite layer with the thickness $d_{mix} = 150$ nm consists of silver nanospheroids suspended in a transparent optical glass. The parameters of silver are $\varepsilon_0 = 5$, $\omega_p = 9$ eV, and $\gamma = 0.02$ eV and the permittivity of glass is $\varepsilon_d = 2.56$. Frequency dependences of the real and imaginary parts of the permittivities for spherical and spheroid particles calculated using formula (1) show that the position of the resonance curve significantly changes with increasing ratio between the lengths of the polar and equatorial semiaxes and the invariable volume concentration of extended spheroids relative to the case of spherical particles. In this case, the half-width of the resonance curve $\varepsilon''_{mix}(\omega)$ changes insignificantly, the curve $\varepsilon'_{mix}(\omega)$ is noticeably modified, and the frequency range with $\varepsilon'_{mix}(\omega) < 0$ is extended. Figure 2a shows the dependences of $\varepsilon'_{mix}(\omega)$ and $\varepsilon''_{mix}(\omega)$ on the normalized frequency for the invariable factor of filling with spherical nanoparticles f = 0.2 ($\xi = 1$). The observed resonance for spheres at the frequency $\omega = 0.2882\omega_p$ (Fig. 2a) with the corresponding wavelength $\lambda = 451.5$ nm is related to the plasmon resonance of nanoparticles [27, 31]. The position of the transmission peak in the band gap of the PC at $\xi = 1$ (Fig. 4) corresponds to the OTS frequency. The obtained OTS exists only in an extremely narrow frequency range where the nanocomposite is similar to a metal (insert to Fig. 2a). At the OTS frequency, the permittivity of the nanocomposite is $\varepsilon'_{mix}(\omega) = -0.3021 + 0.0646i$. At the same frequency, the permittivity of a silver film in Drude approximation (4), which follows from Eq. (1) at the filling factor f = 1, is determined by the expression $\varepsilon = -3.6146 + 0.0562$ i.
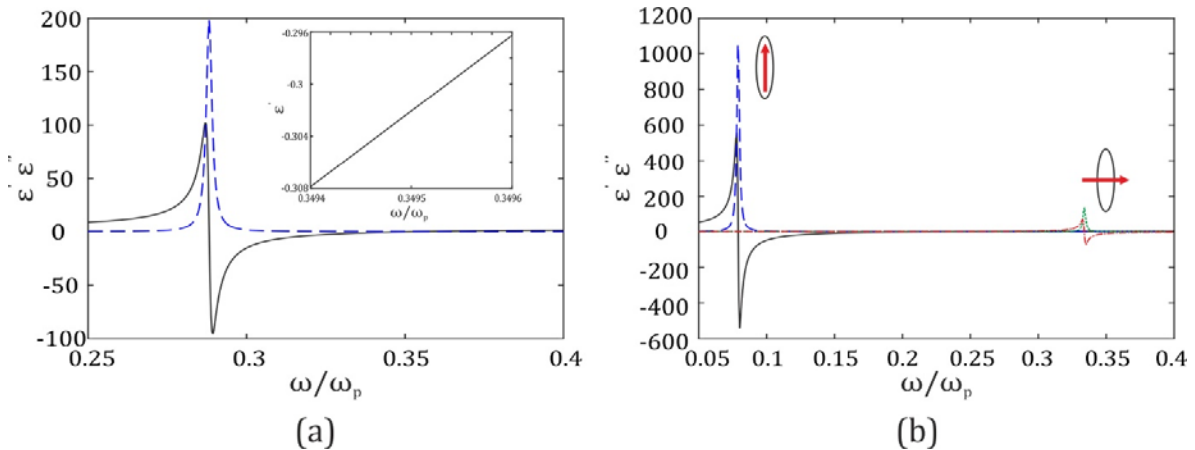

(a)

(b)

Fig. 2. Dependences of the real and imaginary parts of effective permittivity $\varepsilon_{mix}(\omega)$ on normalized frequency ω/ω_p for spherical particles with $\xi = 1$ ($\varepsilon'_{mix}(\omega)$ - solid line, $\varepsilon''_{mix}(\omega)$ – long-dash line) (a) and spheroidal particles with $\xi = 10$ (b). Insert: enlarged values of $\varepsilon'_{mix}(\omega)$ near the frequency corresponding to the Tamm state in Fig. 4. The left peak in Fig. 2b corresponds to the parallel component of the effective permittivity ($\varepsilon'_{mix}(\omega)$ - solid line, $\varepsilon''_{mix}(\omega)$ – long-dash line) and the right peak, to its perpendicular component ($\varepsilon'_{mix}(\omega)$ – dot-dash line, $\varepsilon''_{mix}(\omega)$ – dashed line). The filling factor is f = 0.2.

As the geometry of nanoparticles changes, new resonance peaks arise in the spectrum. Frequencies of these peaks depend on the electric field direction relative to the axis of revolution of the spheroid and on the ratio between the lengths of the polar and equatorial semiaxes of nanoparticles. The difference between the resonance frequencies of permittivities $\varepsilon_\perp$ and $\varepsilon_\parallel$ makes the optical properties of the nanocomposite dependent on polarization of the incident wave. When the nanocomposite is strongly anisotropic ($\xi \gg 1$), the plasmon resonances for the field directed along the spheroid axis appear beyond the visible spectral range. In particular, at $\xi = 10$, the resonances for the parallel and perpendicular components of the permittivity occur at the frequencies $\omega = 0.0789\omega_p$ and $\omega = 0.3338\omega_p$, respectively (Fig. 2b).

The nature of the Tamm state and its relationship to the transmission peak is independently examined by the dispersion equation for the surface and bulk electromagnetic modes. We consider a TM-type wave at the boundary of a semi-infinite PC and an isotropic nanocomposite [32]:

$$(\varepsilon_{mix}{}^2 q_1^2 + \alpha^2 \varepsilon_1^2 F^2)\cos(q_1 d_1)\sin(q_2 d_2) + F(\varepsilon_{mix}{}^2 q_1^2 + \alpha^2 \varepsilon_1^2)\sin(q_1 d_1)\cos(q_2 d_2) +$$

$$+(1-F^2)\varepsilon_{mix}\varepsilon_1 \alpha q_1 \sin(q_1 d_1)\sin(q_2 d_2) = 0, \tag{9}$$

$$F = q_1\varepsilon_2 / q_2\varepsilon_2, \tag{10}$$

where $\varepsilon_{1,2}$ are dielectric constants and $d_{1,2}$ are thicknesses of the PC alternating layers.

$$\alpha = \sqrt{k_x{}^2 - \frac{\omega^2 \varepsilon_{mix}}{c^2}}, q_i = \sqrt{\frac{\omega^2 \varepsilon_i}{c^2} - k_x{}^2}, i = 1, 2., \tag{11}$$

where k_x is the projection of the wave vector on the boundary between two media, ω is the wave frequency, c is the speed of light.

The dispersion relation between ω, k_x and Bloch wave number k_B in semi-infinite layered medium has the form

$$\cos(k_B d) = \cos(q_1 d_1)\cos(q_2 d_2) - 1/2(F + F^{-1})\sin(q_1 d_1)\sin(q_2 d_2), \tag{12}$$

with the lattice constant d = $d_1 + d_2$.

The dispersion equation (12) determines the Bloch wave number k_B along the z-axis direction of the Bloch wave with frequency ω, as well as the x component of the wave vector k. In the case of normal incidence of light on the PC, $k_x = 0$, and the expressions for α and q_i take the form

$$\alpha = i\frac{\omega}{c}\sqrt{\varepsilon_{mix}}, \; q_i = \frac{\omega}{c}\sqrt{\varepsilon_i}, i = 1, 2. \tag{13}$$

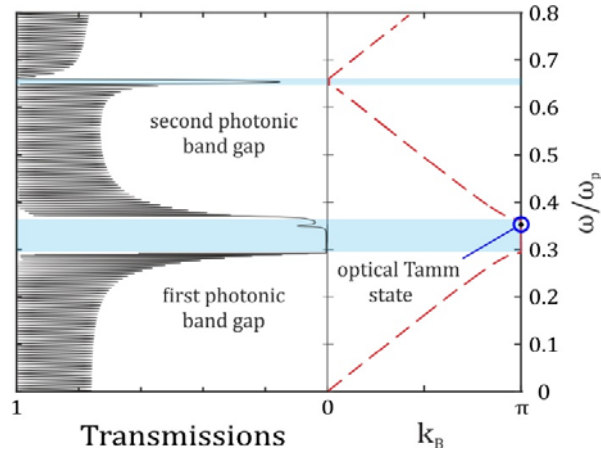The dispersion dependence $\omega(k_B)$ for bulk and surface waves with $k_x = 0$ is shown in Fig. 3.

Fig. 3. Transmissions spectra of the PC obtained by the transfer matrix metod (left) and by dispersion relation ω(k_B) (12) for bulk (long-dash line) and surface electromagnetic modes (indicated by a point), in the case of the normal incidence of light on the PC.

It can be seen that (the results obtained in two different ways completely agree with each other) or (both approaches produce the same result). Namely the same position of the photonic band gaps, their width and position of the OTS at high frequency border of the first bang gap of PC. We can say that the OTS is a particular solution of the dispersion equation (9), in the case of normal incidence of light on the PC. It is formed as a standing surface wave without energy transfer. At the wavelength of the transmission peak the light field is localized at the boundary between the PC and nanocomposite layer and exponentially decrease in either direction. In fact, the light keeps locked between two mirrors - Bragg and metal, since the OTS wavelength falls into the bang gap of the photonic crystal and in the region of negative values of the real part of the nanocomposite effective permittivity.

The dependence of the frequency spectrum on ξ for the field directed perpendicular to the nanocomposite optical axis is shown in Fig. 4.
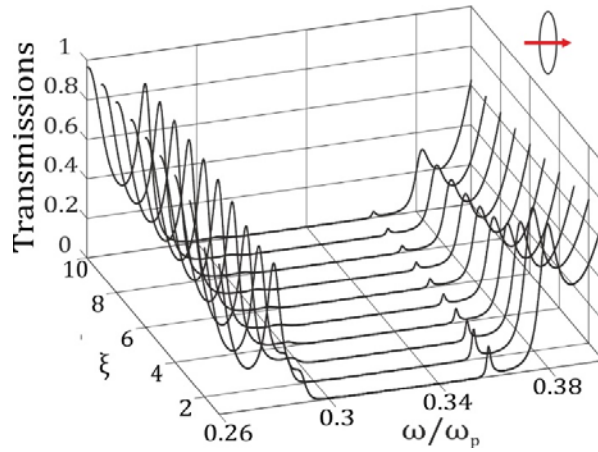

Fig. 4. Transmission spectra at the normal incidence of light onto the PC conjugated with the nanocomposite layer with dispersed spherical ($\xi = 1$) and extended nanoparticles for the field normally polarized with respect to the nanocomposite optical axis. The filling factor is $f = 0.2$ and the nanocomposite layer thickness is $d_{mix} = 150$ nm.

When the electric field vector is normal to the nanocomposite optical axis, the shift of the nanocomosite resonance to the high-frequency region does not significantly modify the frequency spectrum, since the nanocomposite stopband lies within the band gap of the initial crystal. At the given parameters of the system, the OTS is not implemented already at $\xi > 2$ for the parallel component of the effective permittivity. As the ratio between the nanoparticle semiaxes is increased, the nanocomposite band gap shifts toward lower frequencies, which leads to the distortion of the transmission spectrum of the initial PC and complete deformation of the left boundary of the first band gap. This allows obtaining a wide band gap combined from the PC and nanocomposite band gaps. Nanocomposite bang gap is due to the negative dielectric constant $\varepsilon'_{mix}(\omega) < 0$ in the frequency range

from $\omega = 0.0789\omega_p$ to $\omega = 0.2639\omega_p$, which is similar to metallic one. (рис. 2b).Figure 5b show that in the band gap frequency range from $\omega = 0.1\omega_p$ to $\omega = 0.3\omega_p$ the reflection coefficient is equal to 98%. This causes such a broad band gap.

In particular, at the filling factor $f = 0.3$ and the ratio between the semiaxes $\xi = 10$, the combined band gap is 1.77 μm.

The optical Tamm state corresponding to each of the two orthogonal polarizations of the incident wave can be also implemented at large ratios between the spheroid semiaxes. For this purpose, it is necessary to change the PC lattice period, i.e., the position of the PC band gap relative to the resonance frequency of the nanocomposite. It can be seen in Fig. 5 for the longitudinal polarization of the field that, increasing the PC period in the investigated structure with $\xi = 6$, one can obtain the transmission peak corresponding to the OTS near the high-frequency boundary of the PC band gap.

The obtained OTS exists only in an extremely narrow frequency range. At the OTS frequency $\omega = 0.2709\omega_p$, the permittivity of the nanocomposite is $\varepsilon'_{mix}(\omega) = -1.0176 + 0.0381i$.
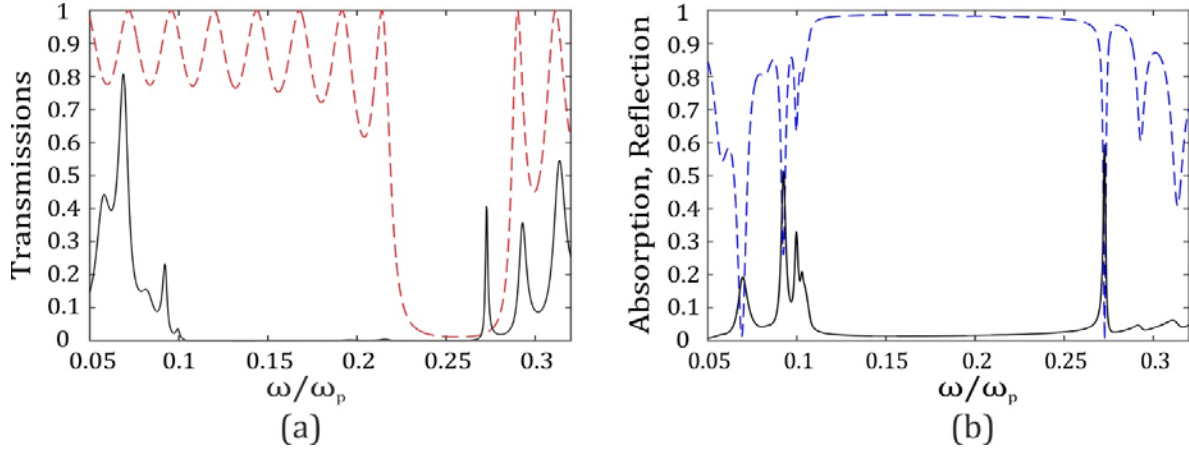

Fig. 5. Transmission spectra for the original PC (dashed line) and for PC bounded by the strongly anisotropic nanocomposite on one side (solid line) (a) and respective absorption (solid line) and reflection (long-dash line) (b). The layer thicknesses are $d_a = 110$ nm and $d_b = 55$ nm, the filling factor is $f = 0.3$, and $\xi = 6$. The rest parameters are the same as used to produce Fig. 2.

The electric field intensity distribution in the sample for the mode with the frequency corresponding to the OTS is illustrated in Fig. 6.
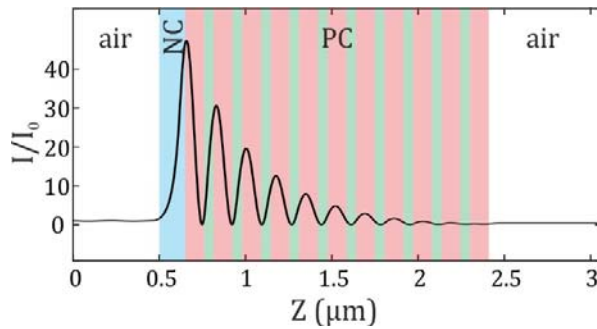

Fig. 6. Schematic of the 1D PC conjugated with the anisotropic nanocomposite layer and field intensity distribution for the parallel polarization of the normally incident light.

It can be seen that the light field in the OTS is localized in the region comparable with the wavelength.

3.2. Bound optical Tamm states

When nanocomposite media bound the photonic crystal on both sides, the transmission spectrum of the structure can contain two transparency bands in the PC band gap.

Figure 7 shows the transmission spectra of the PC structure for the cases when the nanocomposite film is located at one or both boundaries of the PC structure. When there is the contact of the films on both sides of the PC, the optical Tamm modes localized at the interfaces overlap, which eliminates degeneracy; i.e., the frequency splits and two peaks arise in the transmission spectrum in the PC band gap.
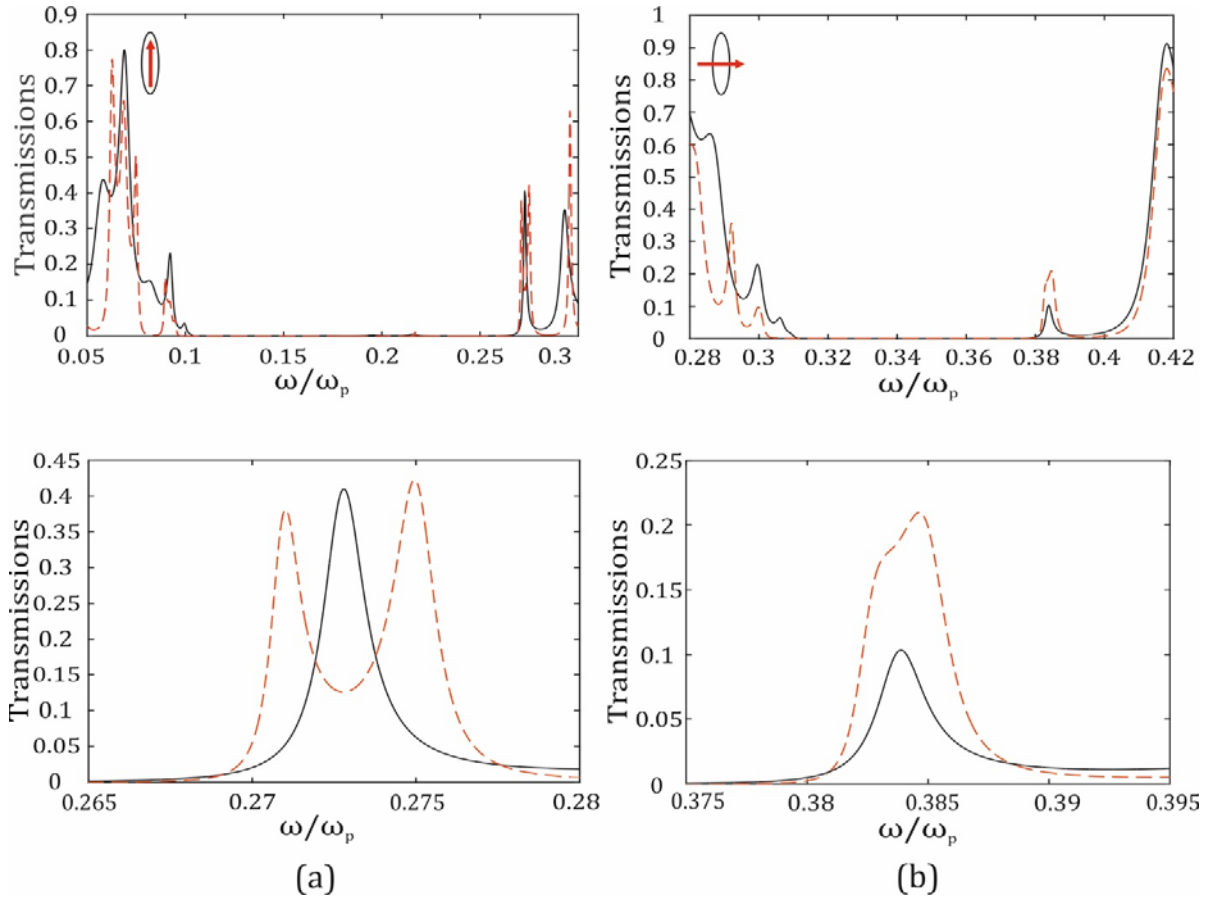
Fig. 7. Transmission spectra of the PC bounded by the strongly anisotropic nanocomposite on one (solid line) and both sides (long-dash line) for (a) the parallel and (b) perpendicular components of the electric field. The nanocomposite layer thickness is 150 nm; (a) $d_a = 110$ nm and $d_b = 55$ nm and (b) $d_a = 74$ nm and $d_b = 40$ nm. The filling factor is $f = 0.3$ and $\xi = 6$.

It should be noted that the interactions between the OTSs are different for different components of the effective permittivity. The most intense interaction and, consequently, splitting of the initial frequency are observed at the parallel polarization of the field. Figure 8 shows the field distribution for the high- and low-frequency transmission peaks from Fig. 7a for the case when the nanocomposite film is located on both sides of the PC.
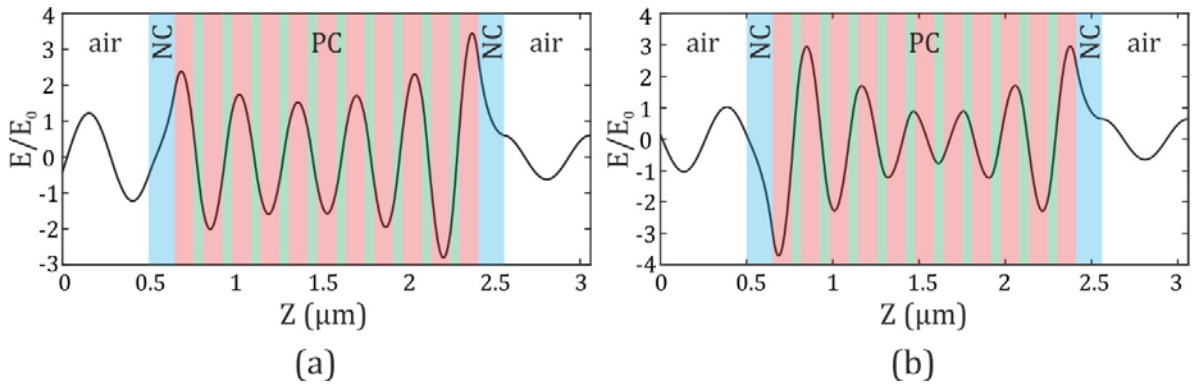
Fig. 8. Schematic of the 1D PC conjugated with the two anisotropic nanocomposite layers and strength of the electric field polarized along the nanocomposite optical axis for (a) low-frequency symmetric and (b) high-frequency antisymmetric optical Tamm modes of the structure.

It can be seen that the coupling of the OTSs localized at the interface between the PC and nanocomposite results in the formation of symmetric and antisymmetric waveguide modes. As the filling factor is increased, the interaction of the OTSs enhances and the splitting of the initial OTS becomes stronger. This is due to the fact that an increase in filling factor f leads to an increase in the length of light field localization in the OTS, which is determined as a distance from the boundary at which the field intensity envelope decreases by a factor of e.

Figure 9 shows transmission spectra for the investigated structure at different filling factors and the rest parameters of the system being invariable. It can be seen in Fig. 9a that the splitting increases with the volume fraction of nanoparticles. In particular, at $f = 0.3$ the splitting is 7.2 nm. However, the calculations show that the splitting decreases with increasing ratio between the polar and equatorial semiaxes.
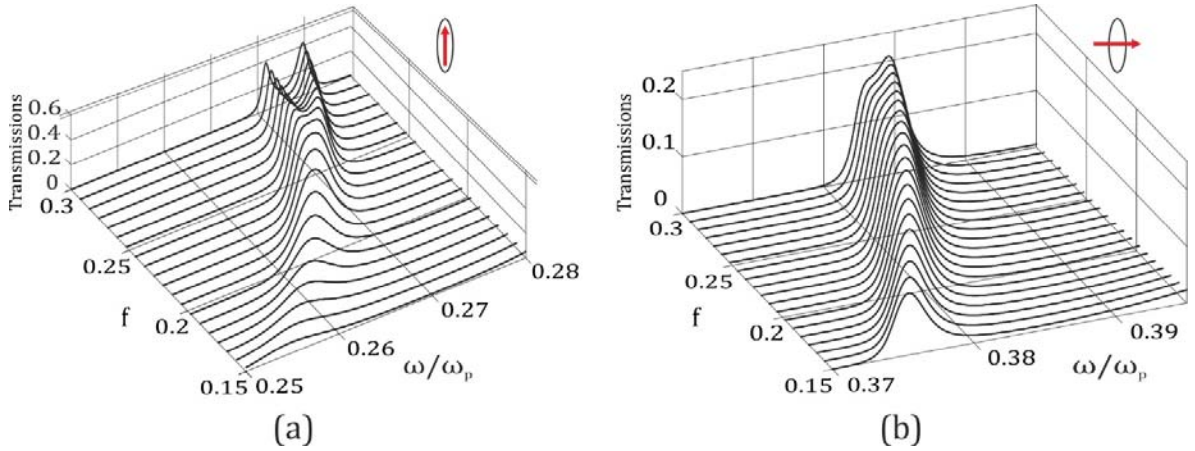

Fig. 9. Transmission spectra of the nanocomposite-PC-nanocomposite structure at different filling factors for (a) parallel and (b) perpendicular polarization of the light field. The system parameters are the same as in Fig. 7.

3.3. Size effect and formation of the OTSs at the interface between the photonic crystal and anisotropic nanocomposite

Previously, the transmission spectra of the nanocomposite-PC system were obtained with disregard of the size effects. For small particles, the size dependence of permittivity caused by the limited conduction electron free path cannot be ignored. To take into account collisions of electrons with the nanoparticle surface, we introduce the addition to the relaxation rate, which is inversely proportional to the polar or equatorial semiaxis [33, 34]

$$\gamma = \gamma_0 + A \frac{\vartheta_{fer}}{r} \tag{14}$$

where γ_0 is the quantity inversely proportional to the electron relaxation time; A is the dimensionless quantity, which lies within $0.4-0.8$ for silver [34]; and ϑ_{fer} is the mean velocity of electrons on the Fermi surface, which amounts to $\vartheta_{fer} = 1.4*10^6$ m/s for silver. Figure 10 show curves of transmission in the PC band gap that correspond to the OTSs at the nanocomposite-PC interface with regard to the size effect for the parallel and perpendicular components of the effective permittivity.
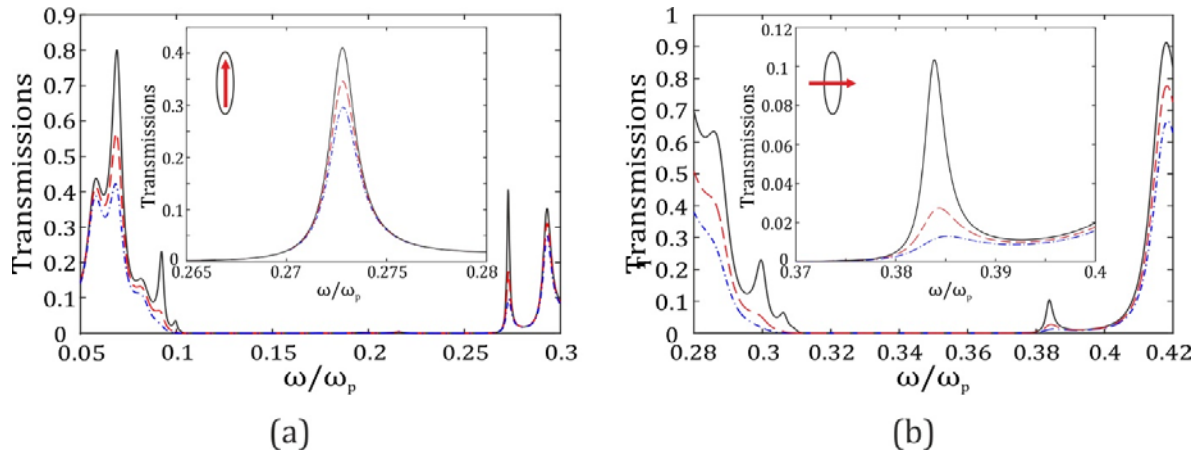
Fig. 10. OTS at the nanocomposite-PC interface with disregard of the size effect (solid line) and with regard to the size effect for particles with the polar and equatorial semiaxes $a = 60$ nm and $b = 10$ nm (long-dash line) and $a = 30$ nm and $b = 5$ nm (dot-dash line) for the parallel component of the effective permittivity (a) and for the perpendicular component of the effective permittivity (b). $\xi = a/b = 6$, A=0.4.

Comparing Fig. 10a and 10b, one can see that the size effect influences stronger the transmission of the light polarized along the equatorial axis of spheroidal particles (Fig. 10b). This is due to the fact that the equatorial semiaxis is shorter than the polar one by a factor of 6 and electrons experience additional scattering on the surface of the metal spheroid along its equator, which, in turn, significant enhances absorption and weakens transmission of light polarized along the equatorial axis at the OTS frequency.

4. CONCLUSIONS

We investigated the spectral properties of the 1D PC bounded on one or both sides by the resonantly absorbing nanocomposite layer consisting of silver nanoparticles with the orientation-ordered spheroidal shape suspended in a transparent optical glass. The results were obtained using the transfer matrix technique. The spectral manifestation of the OTS is caused by the negative effective resonance permittivity of the composite in the visible spectral range.

It was demonstrated that at the strong anisotropy ($\xi \gg 1$), the OTS is implemented only for the transverse polarization of the incident wave. To implement the OTS corresponding to each of the two orthogonal polarizations, one should change the PC lattice period, i.e., the position of the band gap relative to the nanocomposite resonance frequency. It was established that the splitting of modes due to the interaction between the OTSs localized at the interfaces between the PC and nanocomposite increases with increasing volume fraction of nanoparticles, but decreases with increasing ratio between the polar and equatorial semiaxes. It was shown that for particles with $\xi \gg 1$ the size effect plays an important role in the spectral manifestation of the OTS for the field polarized normally to the nanocomposite optical axis. These conclusions are valid also for the flattened spheroids with $\xi \ll 1$, but in this case the longitudinal resonance frequencies are higher than the transverse resonance frequencies.

References

[1]. P. Vinogradov, A. V. Dorofeenko, A. M. Merzlikin, A. A. Lisyansky, Surface states in photonic crystals, Phys. Usp. 53 (2010) 243–256.
[2]. Kavokin, I. Shelykh, and G. Malpuech, Optical Tamm states for the fabrication of polariton lasers, Appl. Phys. Lett. 87 (2005) 261105.
[3]. V. Kavokin, I. A. Shelykh, G. Malpuech, Lossless interface modes at the boundary between two periodic dielectric structures, Phys. Rev. B 72 2005 233102.
[4]. M. Kaliteevski, I. Iorsh, S. Brand, R. A. Abram, J. M. Chamberlain, A. V. Kavokin, and I. A. Shelykh, Tamm plasmon-polaritons: Possible electromagnetic states at the interface of a metal and a dielectric Bragg mirror, Phys. Rev. B 76 2007 165415.
[5]. S. Ya. Vetrov, R. G. Bikbaev, and I. V. Timofeev, Optical Tamm states at the interface between a photonic crystal and a nanocomposite with resonance dispersion," JETP 117 2013 988-998.

[6]. M. E. Sasin, R. P. Seisyan, M. A. Kalitteevski, S. Brand, R. A. Abram, J. M. Chamberlain, A. Yu. Egorov, A. P. Vasil'ev, V. S. Mikhrin, and A. V. Kavokin, Tamm plasmon polaritons: Slow and spatially compact light, Appl. Phys. Lett. 92 2008 251112.

[7]. T. Goto, A. V. Dorofeenko, A. M. Merzlikin, A. V. Baryshev, A. P. Vinogradov, M. Inoue, A. A. Lisyansky, and A. B. Granovsky, Optical Tamm states in one-dimensional magnetophotonic structures, Phys. Rev. Lett. 101 2008 113902.

[8]. W. L. Zhang and S. F. Yu, Bistable switching using an optical Tamm cavity with a Kerr medium, Opt. Comm. 12 2010 2622–2626.

[9]. H. Zhou, G. Yang, K. Wang, H. Long, and P. Lu, Multiple optical Tamm states at a metal-dielectric mirror interface, Opt. Lett. 35 2010 4112.

[10]. P. Vinogradov, A. V. Dorofeenko, S. G. Erokhin, M. Inoue, A. A. Lisyansky, A. M. Merzlikin, and A. B. Granovsky, Surface state peculiarities in one-dimensional photonic crystal interfaces, Phys. Rev. B 74 2006 045128.

[11]. X.-L. Zhang, J.-F. Song, X.-B. Li, J. Feng, and H.-B. Sun, Optical Tamm states enhanced broad-band absorption of organic solar cells, Appl. Phys. Lett. 101 2012 243901.

[12]. Y. Gong, X. Liu, H. Lu, L. Wang, and G. Wang, Perfect absorber supported by optical Tamm states in plasmonic waveguide, Opt. Exp. 19 2011 18393.

[13]. Symonds, G. Lheureux, J.P. Hugonin, J.J. Greffet, J. Laverdant, G. Brucoli, A. Lemaitre, P. Senellart, and J. Bellessa, Confined Tamm plasmons for metal-semiconductor lasers, Nano. Lett. 13 2013 3179.

[14]. O. Gazzano, S. Michaelis de Vasconcellos, K. Gauthron, C. Symonds, P. Voisin, J. Bellessa, A. Lemaîtrе, and P. Senellart, Single photon source using confined Tamm plasmon modes, Appl. Phys. Lett. 100 2012 232111.

[15]. H. Y. Dong, J. Wang, and T. J. Cui, One-way optical tunneling induced by nonreciprocal dispersion of Tamm states in magnetophotonic crystals, Phys. Rev. B 87 2013 045406.

[16]. H. Da, Q. Bao, R. Sanaei, J. Teng, K. P. Loh, F. J. Garcia-Vidal, and C.-W. Qiu, Monolayer graphene photonic metastructures: Giant Faraday rotation and nearly perfect transmission, Phys. Rev. B 88 2013 205405.

[17]. N. E. Khokhlov, A. R. Prokopov, A. N. Shaposhnikov, V. N. Berzhansky, M. A. Kozhaev, S. N. Andreev, Ajith P. Ravishankar, Venu Gopal Achanta, D. A. Bykov, A. K. Zvezdin and V. I. Belotelov, Photonic crystals with plasmonic patterns: novel type of the heterostructures for enhanced magnetooptical activity, Appl. Phys. 48 2015 095001.

[18]. M Kaliteevski, S Brand, R A Abram, I Iorsh, A V Kavokin, and I A Shelykh, Hybrid states of Tamm plasmons and exciton polaritons, Appl. Phys. Lett. 95 2009 251108.

[19]. R. Brückner, M. Sudzius, S. I. Hintschich, H. Fröb, V. G. Lyssenko, M. A. Kaliteevski, I. Iorsh, R. A. Abram, A. V. Kavokin, and K. Leo, Parabolic polarization splitting of Tamm states in a metal-organic microcavity, Appl. Phys. Lett. 100 2012 062101.

[20]. Afinogenov, V. O. Bessonov, A. A. Nikulin, and A. A. Fedyanin, Observation of hybrid state of Tamm and surface plasmon-polaritons in one-dimensional photonic crystals, Appl. Phys. Lett. 103 2013 061112.

[21]. M.A. Kaliteevski and A. A. Lazarenko, Reduced absorption of light by metallic intra-cavity contacts: Tamm plasmon based laser mode engineering, Tech. Phys. Lett. 39 2013 698.

[22]. J. Gessler, V. Baumann, M. Emmerling, M. Amthor, K. Winkler, S. Höfling, C. Schneider, and M. Kamp, Electro optical tuning of Tamm-plasmon exciton-polaritons, Appl. Phys. Lett. 105 2014 181107.

[23]. R. S. Savelev, A. E. Miroshnichenko, A. A. Sukhorukov, Y. S. Kivshar, "Optical Tamm states in arrays of all-dielectric nanoparticles," JETP Lett. 100 2014 430.

[24]. V. Treshin and V. V. Klimov, Optical Tamm state and extraordinary light transmission through a nanoaperture, Phys. Rev. A 88 2013 023832.

[25]. S. Ya. Vetrov, M. V. Pyatnov, I. V. Timofeev, Surface modes in "photonic cholesteric liquid crystal–phase plate–metal structure, Opt. Lett. 39 2014 2743-2746.

[26]. J.C. Maxwell Garnett, Colours in Metal Glasses, in Metallic Films, and in Metallic Solutions. II (Philosophical Transactions of the Royal Society of London, 1904.

[27]. S.G. Moiseev, Nanocomposite-based ultrathin polarization beamsplitter, Opt. Spectr. 111 2011 264.

[28]. D.Wang, S. Guo, S. Yin, Surgeon Maturin, Opt.Eng. 42 2003 3585.

[29]. S.D. Stookey, R.J. Aranjo Selective polarization of light due to absorption by small elongated silver particles in glass, J. Appl. Opt. 7 1968 777.

[30]. P. Yeh, Electromagnetic propagation in birefringent layered media, J. Opt. Soc. Am. 69 1979 742–756.

[31]. Sihvola, Electromagnetic Mixing Formulas and Applications. Institution of Engineering and Technology, London, 2008.

[32]. H. Shi, Ch. Tsai, Solid State Comm. 52 1984 953.

[33]. S.G. Moiseev, V.A. Ostatochnikov, and D.I. Sementsov, Influence of size effects on the optical characteristics of a one-dimensional photonic crystal with a nanocomposite defect, JETP Lett. 100 2014 413-417.

[34]. V.V. Klimov, Nanoplasmonics, P. N. Lebedev Physical Institute, 2009